Solid State Ionics 245-246 (2013) 49–55

Contents lists available at SciVerse ScienceDirect

Solid State Ionics

journal homepage: www.elsevier.com/locate/ssi

# A highly safe and inflame retarding aramid lithium ion battery separator by a papermaking process ☆

Jianjun Zhang [a], Qingshan Kong [a], Zhihong Liu [a], Shuping Pang [a], Liping Yue [a,b], Jianhua Yao [a], Xuejiang Wang [a], Guanglei Cui [a,*]

[a] Qingdao Key Lab of solar energy utilization and energy storage technology, Qingdao Institute of Bioenergy and Bioprocess Technology, Chinese Academy of Sciences, Qingdao 266101, China
[b] College of Chemistry and Molecular Engineering, Qingdao University of Science and Technology, Qingdao 266042, China

ARTICLE INFO

*Article history:*
Received 9 November 2012
Received in revised form 24 May 2013
Accepted 24 May 2013
Available online xxxx

*Keywords:*
Inflame retarding
Aramid
Separator
Lithium ion battery
Papermaking

ABSTRACT

An aramid membrane with good electrolyte wettability, high ionic conductivity, excellent inflame retarding property and superior thermal resistance has been successfully fabricated via a facile papermaking process for improving the safety characteristic of lithium ion battery. The aramid membrane endows the lithium cobalt oxide ($LiCoO_2$)/graphite cell superior cycle performance and better interfacial flexibility. In addition, the lithium iron phosphate ($LiFePO_4$)/lithium cell using such aramid membrane exhibited stable charge–discharge profiles and satisfactory cycling stability even at an elevated temperature of 120 °C. These fascinating characteristics and facile papermaking method provide potential application as separator in high energy lithium ion battery.



## 1. Introduction

Due to its high energy and power characteristics, lithium ion battery has attracted extensive attention for high-power tools and portable electronic applications [1–7]. Lithium ion battery separator plays a determinant role in safety issues, which is to allow fast transport of ionic charge and prevent electrical short circuits between cathode and anode. Currently, most commercial separators in lithium ion battery are typically made of polyolefin materials, such as polyethylene (PE), polypropylene (PP) and their blends. These separators possess many advantages such as electrochemical stability, proper mechanical strength and thermal shutdown properties [8–10]. However, their poor thermal shrinkage, low porosity and inferior electrolyte wettability have often aroused some serious concerns about their future application in electric vehicles, as far as safety issues and long-term application of electric vehicles is concerned. Since commercial polyolefin separators might thermally runway in case of malfunction of the battery, highly safe separators must be urgently explored. Remarkable efforts have been invested to solve the aforementioned challenges, which include the coating of nanoparticles to enhance interfacial stability [11–15] and exploring the nanofiber nonwovens [16–23]. Unfortunately, the problem of unbounded inorganic nanoparticles still exists and the latter normally suffers from poor mechanical strength. In addition, polyolefin as scaffold still suffer from thermally runaway risks owing to a poor thermal resistance. So it is obligatory for us to find out a promising technique for the fabrication of robust and highly safe separator.

Most of the commercially available polyolefin separators are made of PE, PP or their mixtures through either dry or wet process [10,24]. Both processes include an extrusion step to make thin films and employ one or more orientation steps to impart porosity and increase the tensile strength. Separators made by the dry process generally undergo thermal shrinkage along the machine direction at elevated temperature, while those prepared by the wet process exhibit relative high cost. The most widely used processes for manufacturing nonwoven separator are electrospinning method and melt-blown technology. [25–27]. Non-woven separators produced by electrospining method are featured by a high porosity and uniform pore size. However, this kind of membrane shows low mechanical strength. Separators made by melt-blown technology exhibits good mechanical properties, but it suffered from excessively large-sized pores, which was not beneficial to maintain the battery voltage due to self-discharge and also vulnerable to breakdown at high discharge rates or under vigorous conditions. Microporous polymer membrane was also obtained by phase inversion process [28,29], which requires a lot of organic solvent and then generates extra cost. It is well known that papermaking technique has been demonstrated to be an efficient procedure to fabricate nonwoven membrane. The preparation of bamboo fiber and PP composite membrane was carried out



* Corresponding author. Tel.: +86 532 80662746; fax: +86 532 80662744.
*E-mail address:* cuigl@qibebt.ac.cn (G. Cui).

0167-2738/$ – see front matter © 2013 The Authors. Published by Elsevier B.V. All rights reserved.
http://dx.doi.org/10.1016/j.ssi.2013.05.016

via papermaking method to solve the dispersion problem of bamboo fiber [30]. It was also proved that papermaking technology is an effective way to achieve large-scale production of composite membrane [31,32]. Aramid possessing excellent mechanical properties, inflame retarding, superior heat resistance and electric insulating property are widely used as high temperature filter material, electrical insulation and high-temperature protective clothing [33–36]. It is expected that aramid lithium ion separator could deliver a superior thermal resistance, inflame retarding and high safety characteristic especially for electrical vehicle applications [37]. So far, there is rare report on exploring aramid membrane as lithium ion battery separator via a papermaking process. Herein, a major objective of this work is to explore aramid membrane as highly safe lithium ion battery separator. It is demonstrated that such membrane exhibits desirable heat resistance, excellent electrochemical stability and good battery performance, which render aramid membrane the feasibility to serve as a promising separator for high energy lithium ion battery.

## 2. Experimental

### 2.1. Materials

Aramid short fibers and aramid pulps were purchased from DuPont Company. PP separator (Celgard 2500) was purchased from Celgard Company. Other chemical reagents were all purchased commercially and used without further purification.

### 2.2. Preparation of the aramid membrane

A schematic illustration for preparation of the aramid membrane was shown in Fig. 1. The aramid short fibers (146 g) and aramid pulps (219 g) were soaked with 20 L water and pulped for 2 h to form completely dispersed fiber suspension, then the wet aramid sheet was made on a papermaking machine. The formed wet sheet was transferred to a plate dryer to remove additional water. Hot calendering was further carried out, which temperature and pressure was set to 240 °C and 14 MPa, respectively. The final aramid membrane was dried under vacuum at 50 °C for 24 h.

We can fabricate aramid membrane with different thickness by adjusting the grammatura ($g/m^2$). For example, we obtained aramid membrane with 75 μm when the grammatura was 35 $g/m^2$. Correspondingly, we can prepare membrane with different thickness by adjusting the grammatura.

### 2.3. Membrane characterization

The surface morphology of separators was observed by a Hitachi S-4800 field emission scanning electron microscope (SEM) [38]. The porosity of the separators can be measured using n-butanol absorption method [39]. For this purpose, the mass of the separators was measured before and after immersion in n-butanol for 2 h. The porosity of the membrane was calculated using the equation: porosity $= (m_b / \rho_b) / (m_b / \rho_b + m_p / \rho_p) \times 100\%$, where $m_b$ and $m_p$ are the mass of n-butanol and the separator and $\rho_b$ and $\rho_p$ are the density of n-butanol and the separator, respectively. For example, we used density of PP material to calculate the porosity of PP separator. Meanwhile, we used density of aramid material to calculate the porosity of aramid membrane. The air permeability of the separators was examined with a Gurley densometer (4110 N, Gurley) by measuring the time for air to pass through a determined volume (100 cc) [40]. The electrolyte uptake was obtained by measuring the weight of separators before and after liquid electrolyte soaking for 2 h and then calculated using following equation: electrolyte uptake $= (W_f - W_i) / W_i \times 100\%$, where $W_i$ and $W_f$ are the weights of the separator before and after soaking in the liquid electrolyte, respectively [41].

The mechanical property was measured using an Inston-3300 universal testing machine (USA) at a stretching speed of 1.66 mm $s^{-1}$ with the sample straps of about 1 cm wide and 8 cm long [42]. To evaluate its thermal shrinkage behavior, the separators were placed in an oven and heated at 250 °C for 0.5 h [43]. Thermal resistance of the separators was examined by a differential scanning calorimeter (Diamond DSC, PerkinElmer) in a temperature range from 50 °C to 300 °C at a heating rate of 10 °C $min^{-1}$ under nitrogen atmosphere [44]. Limiting oxygen index (LOI) measurements were undertaken using a JF-3 type instrument (China). Specimens of dimensions 100 mm × 100 mm × 10 mm were used for the LOI tests [45]. The specimens of LOI tests were prepared as follows: First, we tailored aramid membrane to form a certain size (1600 mm × 800 mm × 0.075 mm) of the membrane; and second, we fold obtained membrane four times in the length direction and then fold three times in the width direction to get aramid specimen of dimensions 100 mm × 100 mm × 10 mm. The preparation process of PP specimen was using the similar method.

### 2.4. Cell assembly and performance characterization

The electrochemical stability window of the separator was determined by a linear sweep voltammetry experiment at the potential range between 2.5 V and 6.0 V under the scan rate of 1.0 mV · $s^{-1}$ at room temperature [46]. The ionic conductivity of the liquid electrolyte-soaked separator between two stainless-steel plate electrodes was evaluated using the electrochemical impedance spectroscopy (EIS) measurement by applying an AC voltage of 20 mV amplitude in the frequency range of 1 Hz–$10^6$ Hz [47]. A unit cell (2032-type coin) was composed of a $LiCoO_2$ cathode ($LiCoO_2$/carbon black/PVDF 90/5/5 w/w/w), a natural graphite anode (natural graphite/carbon black/CMC/SBR 93/5/1.25/0.75 w/w/w/w), separator and 1 M $LiPF_6$/EC + DEC (1:1 in volume) electrolyte. All assembly of cells was carried out in an argon-filled glove box. For comparison, cells using the PP separator (Celgard 2500) were assembled and tested under the same condition. The discharge current densities were varied from 0.2 C (24 mA $g^{-1}$) to 4.0 C (480 mA $g^{-1}$) under a voltage range between 2.75 V and 4.20 V. The cells were cycled at a fixed charge–discharge current density of 0.5 C/0.5 C for cycle life testing [48].

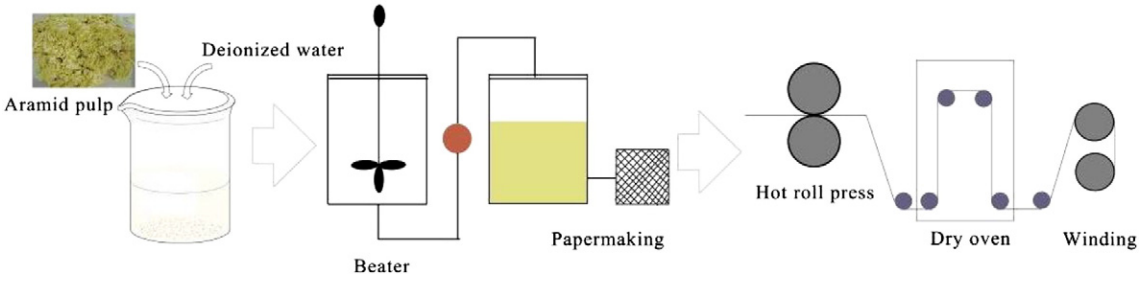


**Fig. 1.** A schematic illustration for preparation of aramid membrane.

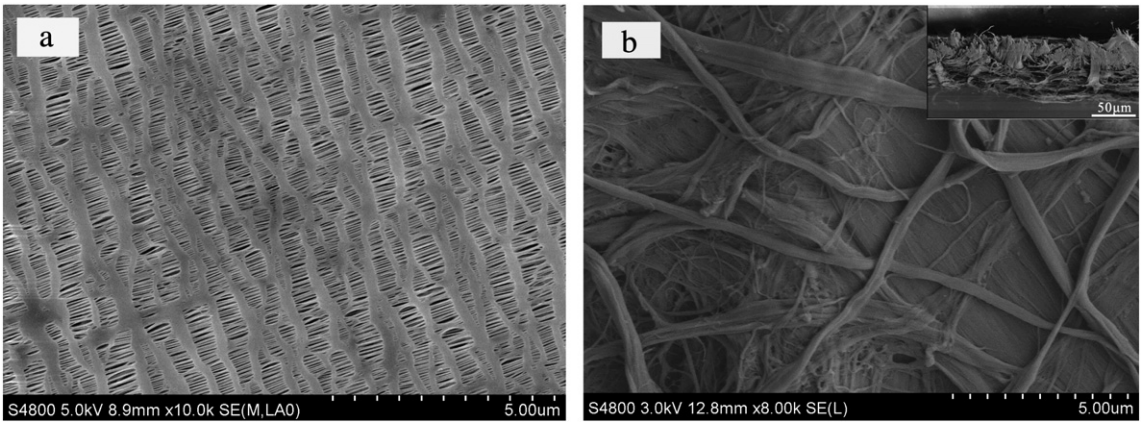


**Fig. 2.** Typical SEM images of (a) PP separator and (b) aramid membrane.

*2.5. Cycling performance of PP separator and aramid membrane at room temperature and elevated temperature*

A coil cell (2032-type) was assembled by sandwiching a separator between a lithium metal foil anode and a $LiFePO_4$ cathode and then filling liquid electrolyte. The $LiFePO_4$ electrode was prepared by a doctor-blading and the mass ratio of $LiFePO_4$/carbon black/PVDF was 80/10/10 (w/w/w). Cycling performance of the cells was examined using a LAND battery testing system at room temperature and 120 °C. The cells were cycled at a fixed charge/discharge current density of 0.5 C (65 mA $g^{-1}$)/0.5 C (65 mA $g^{-1}$) for cycle life testing under a voltage range between 2.5 V and 4.0 V [49].

## 3. Results and discussion

*3.1. Morphological and physical characterization*

The morphology of PP separator and aramid membrane was shown in Fig. 2. It was observed in Fig. 2(a) that the PP separator possessed uniform and typically elliptic pores, which were formed via a uniaxially stretching technology. The long axis of the pore was 100–500 nm and the short axis of about 50 nm. It was presented in Fig. 2(b) that aramid short fibers were homogeneously distributed and the diameter ranged from 1 μm to 5 μm. The inset image in Fig. 2(b) showed the cross section of aramid membrane. The thickness of the aramid membrane was about 75 μm. In addition, aramid membrane was nonwoven membrane, which possessed a three-dimensional porous network structure and highly tortuous pores. This well-interconnected microporous structure and the intrinsically lyophilic nature of aramid material is beneficial to absorb more electrolyte and allow lithium ions transport resulting in high ionic conductivity [50]. Moreover, aramid pulp was wrapped around the fibers to form robust structure, which was beneficial to improve the mechanical strength [43]. These fascinating characteristics were vital to improve cycling performance and safety characteristics of lithium ion battery [38,49].

The thickness, porosity, air permeability and electrolyte uptake of the separators were summarized in Table 1. The Gurley value of the aramid membrane was 13.6 s, which was much lower than that of the PP separator (235 s). It was reported that highly porous structure of the aramid membrane gave rise to lower Gurley value [51], which agreed well with the morphology observation. This microporous structure of the aramid membrane can also be confirmed in the term of better porosity (70%) than that of PP separator (55%). For an ideal separator, high porosity is required to hold sufficient liquid electrolyte for the ionic conductivity between the electrodes.

As we all know, separators of lithium ion battery should be wetted easily and accessible to retain the electrolyte [52]. The liquid electrolyte wettability of PP separator and aramid membrane were vividly shown in Fig. 3. The wettability of PP separator with carbonate electrolyte was poor, due to its hydrophobic surface characteristic and low surface energy [53,54]. The intrinsically hydrophobic nature of polyolefin-based separators and polar electrolyte often led to dry zone in the batteries, which was detrimental to cycle performance of the battery. It was observed that the aramid membrane could be quickly wetted by the liquid electrolyte and its electrolyte uptake became saturated within 10 s. Furthermore, the electrolyte uptake of aramid membrane was 240%, which was double as much as that of PP separator (120%). This superior liquid electrolyte wettability might be attributed to more porous structure and superior interfacial compatibility of the aramid membrane. Higher porosity, lower Gurley value and better wettability of aramid membrane are beneficial to improve the cell performance.

The stress–strain curves of the aramid membrane were depicted in Fig. 4. The maximum stress was 31 MPa, and the deformation was 8.2% in dry state. In order to further evaluate its mechanical property inside the battery, the stress of the aramid membrane was also measured in wet state after being soaked in the liquid electrolyte

**Table 1**
Physical properties of the separators.

| Sample | Thickness (μm) | Porosity (%) | Gurley value (s/100 cc) | Electrolyte uptake (%) | LOI (%) |
|---|---|---|---|---|---|
| PP separator | 25 | 55 | 235 | 120 | 18 |
| Aramid membrane | 75 | 70 | 13.6 | 240 | 28 |

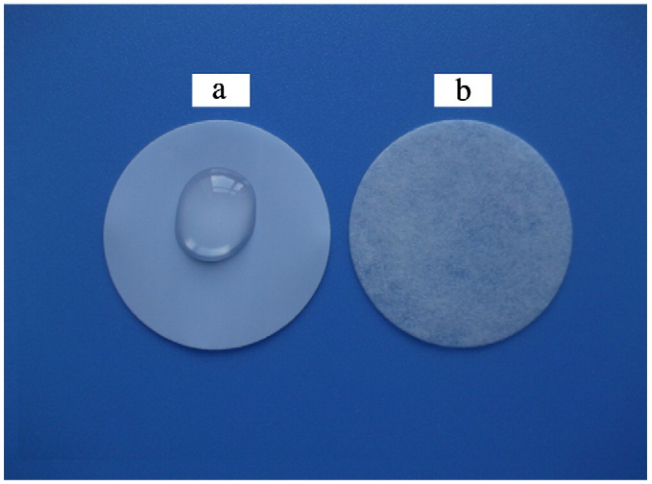


**Fig. 3.** Photographs showing liquid electrolyte wetting behavior of (a) PP separator and (b) aramid membrane.

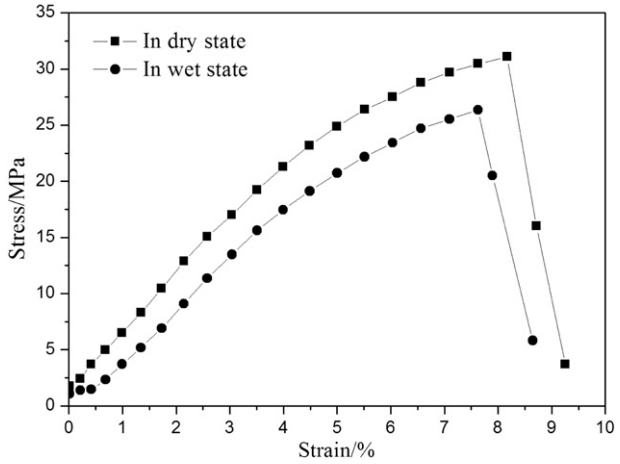


**Fig. 4.** Stress–strain curves of the aramid membrane in dry and wet states.

for 2 h. It was found that the aramid membrane in wet state exhibited reduced tensile strength of 26 MPa and deformation of 7.7%, which was still much higher than the transverse strength (12 MPa) of the PP separator [55]. It was deduced that aramid membrane could reduce the possibility of the mechanical rupture of the membrane and improve the safety characteristics of the lithium ion battery.

### 3.2. Thermal analysis and inflame retarding properties

Thermal properties of the PP separator and aramid membrane were shown in Fig. 5. An endothermic peak at 165 °C for PP separator was assigned to glass transition temperature ($T_g$) of the PP. It was observed that aramid membrane showed no obvious endothermic peak below 300 °C, which agreed well with the reported value in previous literature [56]. This implied that the aramid membrane possessed better thermal stability than PP separator.

Thermal shrinkage of the separators was another important issue pertaining to both battery performance and safety characteristic. Fig. 6 demonstrated the photographs of PP separator and aramid membrane after thermal treatment at 120 °C and at 250 °C for 0.5 h. For a fair comparison, the photographs of 3PP separator and aramid membrane after thermal treatment at 120 °C and at 250 °C for 0.5 h were displayed, respectively. As shown in Fig. 6, aramid membrane exhibited minor dimension shrinkage as compared to PP separator, which also indicated the thermal stability of aramid membrane was significantly better than that of PP separator. It was well known that superior thermal resistance could effectively prevent internal electrical short circuit and endow a better safety characteristic at elevated temperature when the battery was subjected to high charges/discharged rates [57].

Limiting oxygen index (LOI) is a parameter for evaluating flame retardancy and flammability of polymeric materials [58]. LOI corresponds to the minimum percentage of oxygen needed for the combustion of specimens in an oxygen/nitrogen atmosphere. The higher the value of LOI, the better the flame retardancy [59]. The LOI results for the samples were depicted in Table 1. It can be seen that the aramid membrane presented higher LOI values (28%) than that of PP separator (18%). The inflame retarding property of aramid membrane was superior to that of PP separator, which could be due to chemical structure of the aramid membrane [60]. The superior inflame retarding property of aramid membrane could significantly improve the safety characteristics of lithium ion battery.

### 3.3. Electrochemical stability

Electrochemical window, an important parameter to evaluate the electrochemical stability of the separator, was analyzed using a linear sweep voltammetry (LSV) as shown in Fig. 7. It was displayed that carbonate electrolytes soaked PP separator possessed a decomposition voltage around 4.6 V *vs.* $Li^+/Li$, which agreed with the previous literatures [61,62]. In comparison, the current onset of carbonate electrolytes soaked aramid membrane was detected around 5.0 V versus $Li^+/Li$, which was attributed to superior interfacial compatibility of aramid membrane than that of PP in the same electrolyte.

Arrhenius plots of ionic conductivity of liquid electrolyte-soaked PP separator and aramid membrane on the temperature ranged from 30 °C to 90 °C were shown in Fig. 8. At 30 °C, the obtained ionic conductivity was 0.64 mS $cm^{-1}$ and 1.1 mS $cm^{-1}$ for PP separator and aramid membrane, respectively. The enhancement in ionic conductivity could be ascribed to better electrolyte uptake and interaction with polar surface of aramid membrane. High ionic conductivity of aramid membrane is beneficial to improve rate capability of the battery. Taking into account other factors, such as physical property, electrochemical stability and thermal resistance, aramid membrane would be more beneficial to the performance of the cells.

### 3.4. Battery performances

Typical charge–discharge curves at 0.5 C for the $LiCoO_2$/graphite cell using aramid membrane were shown in Fig. 9. Normal and stable discharge profiles were observed in the aramid membrane. In addition, coulombic efficiency of the cell using aramid membrane was 99%. The stable voltage profiles and reasonable coulombic efficiency would be mainly attributed to the electrochemical stability of the aramid membrane.

We further examined the rate capabilities of the $LiCoO_2$/graphite cells using PP separator and aramid membrane. As shown in Fig. 10(a), the specific discharge capacities of the $LiCoO_2$/graphite cell using this aramid membrane were 146 mAh $g^{-1}$, 139 mAh $g^{-1}$ and 118 mAh $g^{-1}$ correspondingly at different rates of 0.2 C, 0.5 C and 1 C, which were much better than those of PP separator. However, when at rate of 2 C and 4 C, the rate performance of battery using aramid membrane was worse than that of battery using PP separator. As mentioned above, the thickness of aramid membrane was 75 μm. It is a common sense that too thick separator was not beneficial to the rate capabilities of the battery. For a fair comparison, we adopted three layers of PP separator. Obviously, rate performance of the battery with three layers of PP separator was much worse than that of battery using aramid separator with same thickness. It is no doubt that the rate capabilities of the aramid membrane needs to be further improved from the viewpoint of practical application, which will be a major research interest in our future studies.

The cycling performance of the $LiCoO_2$/graphite cells assembled with the PP separator and aramid membrane were also investigated.

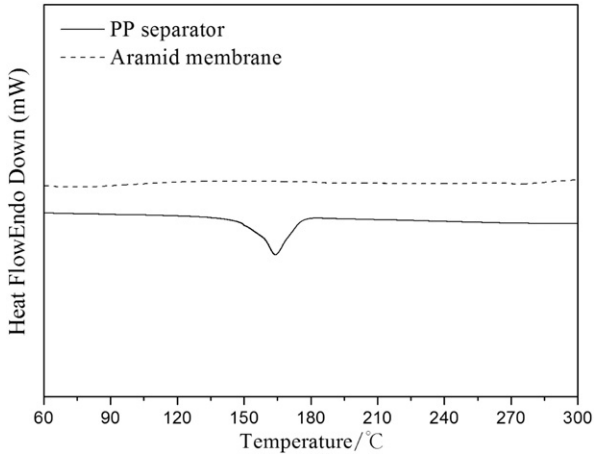


**Fig. 5.** DSC curves of PP separator and aramid membrane.

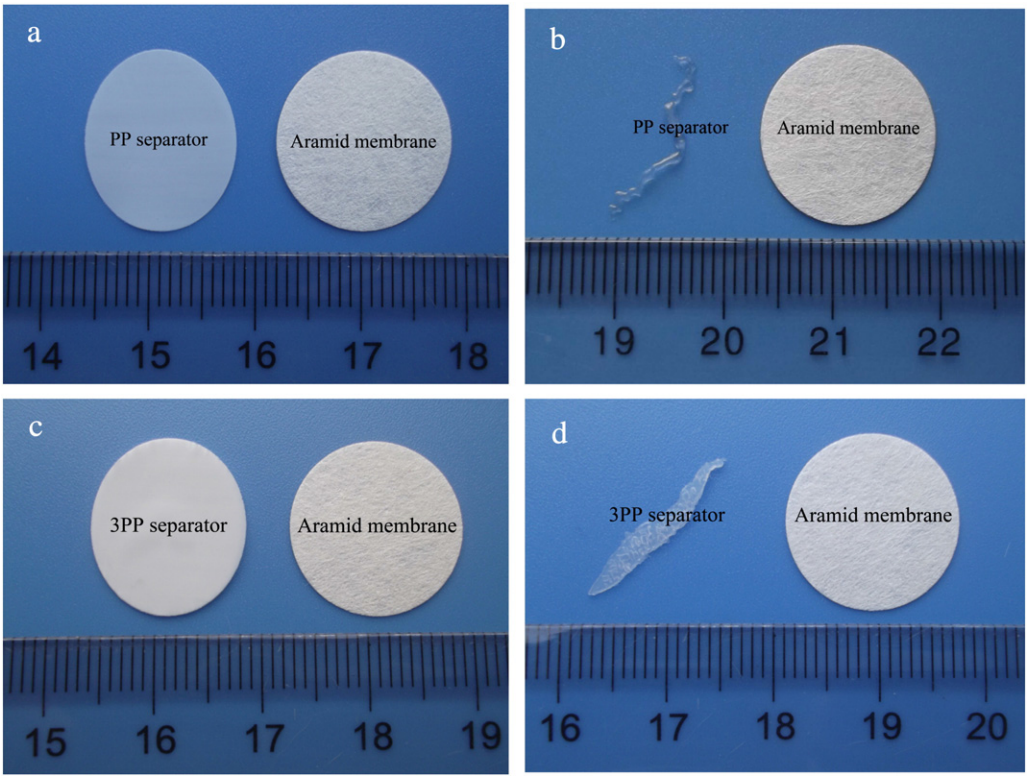


**Fig. 6.** The photographs of PP separator and aramid membrane after thermal treatment (a) at 120 °C and (b) at 250 °C for 0.5 h; the photographs of 3PP separator and aramid membrane after thermal treatment (c) at 120 °C and (d) at 250 °C for 0.5 h.

Fig. 10(b) showed that the discharge capacity retention of the $LiCoO_2$/graphite cells using PP separator and aramid membrane after 100 cycles was 70.2% and 85.2%, respectively. This superior cycling performance of aramid membrane would be ascribed to better liquid electrolyte retention and superior electrochemically interfacial compatibility.

### 3.5. Cycling performance of separators at room temperature and elevated temperature

Typical cycling performance of $LiFePO_4$/Li cells using PP separator and aramid membrane at room temperature was shown in Fig. 11(a). The result showed that the discharge capacity of the cell using aramid membrane was kept at 129 mAh $g^{-1}$ after 100 cycles, showing better capacity retention ratio than that of $LiFePO_4$/Li cell. As a separator feasible for practical applications, it is very required because it not only provides low capacity fading at room temperature but also possesses high capacity retention at elevated temperature [49,57]. $LiFePO_4$ was reported to be a cathode material, which presented better performance even at elevated temperature [63,64]. Fig. 11(b) compared the cycling performance of the $LiFePO_4$/Li cells using PP separator and aramid membrane at 120 °C, respectively. In our experiment, the LiFePO4/Li cell using PP separator would be placed in the oven at 120°C for 2 h before performing cycling performance. It can be seen in Fig. 11(b) that the $LiFePO_4$/Li cell using PP separator could

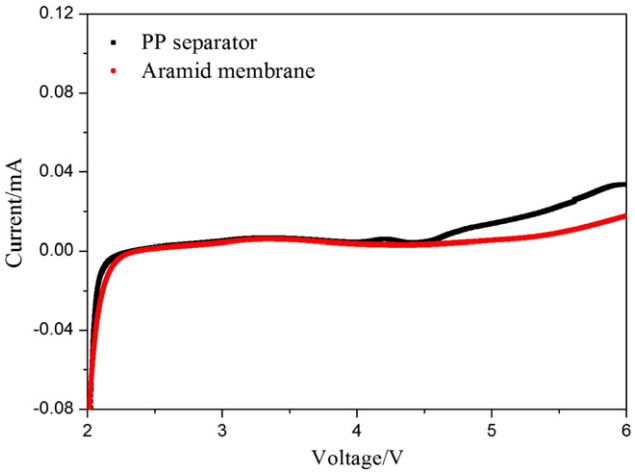


**Fig. 7.** Electrochemical stability of PP separator and aramid membrane.

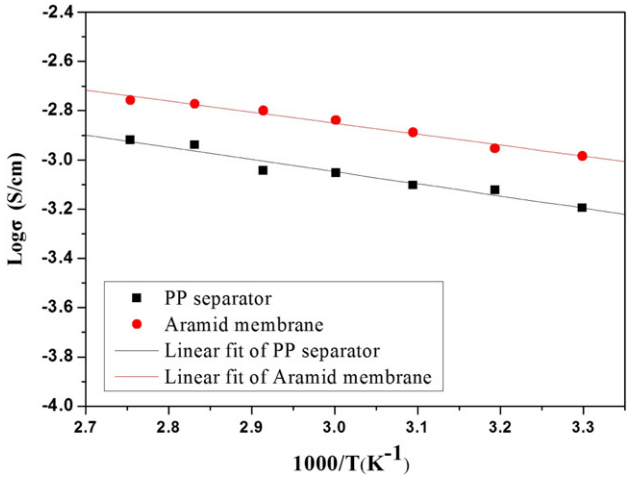


**Fig. 8.** Arrhenius plots of ionic conductivity of liquid electrolyte-soaked PP separator and aramid membrane.

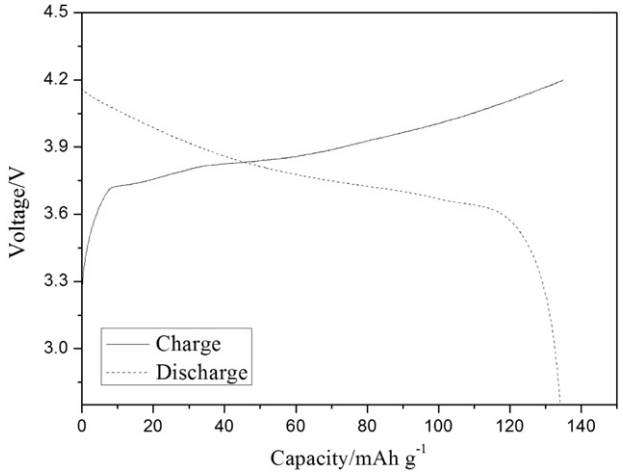


**Fig. 9.** Charge–discharge curves for the $LiCoO_2$/graphite cell using aramid membrane at a rate of 0.5 C.

not even be stably charged and discharged at the temperature. This could be explained by the thermal shrinkage of the PP separator that could cause internal short circuits in the cell at elevated temperature. In contrast, the $LiFePO_4$/Li cell using aramid membrane can

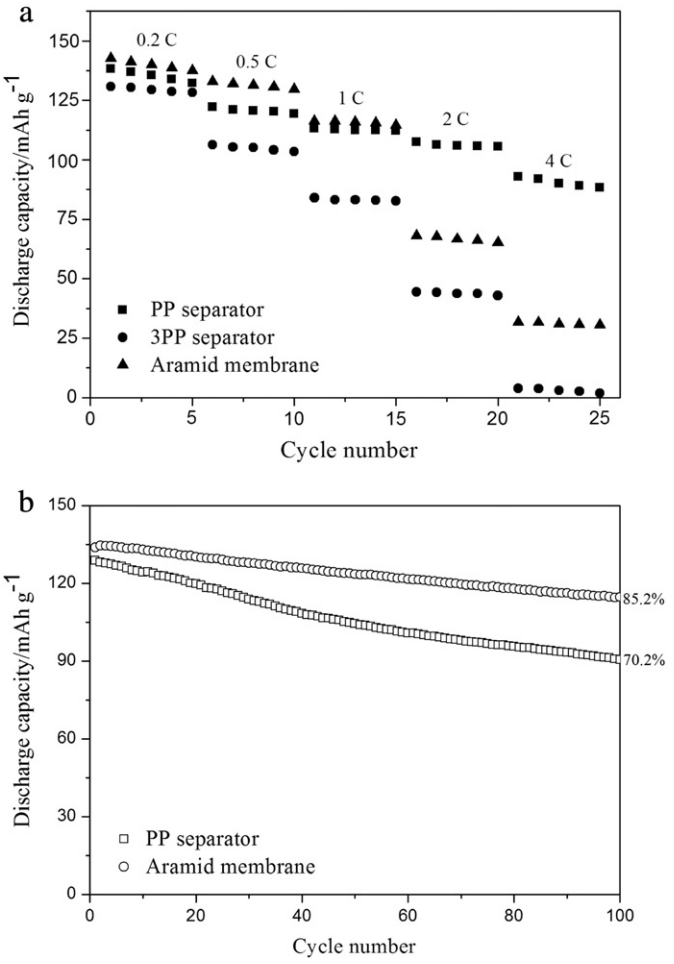


**Fig. 10.** (a) Rate capability of the $LiCoO_2$/graphite cells using PP separator, 3PP separator and aramid membrane. The n in "nPP" means the number of separator layers. (b) Cycle performance of the $LiCoO_2$/graphite cells using PP separator and aramid membrane.

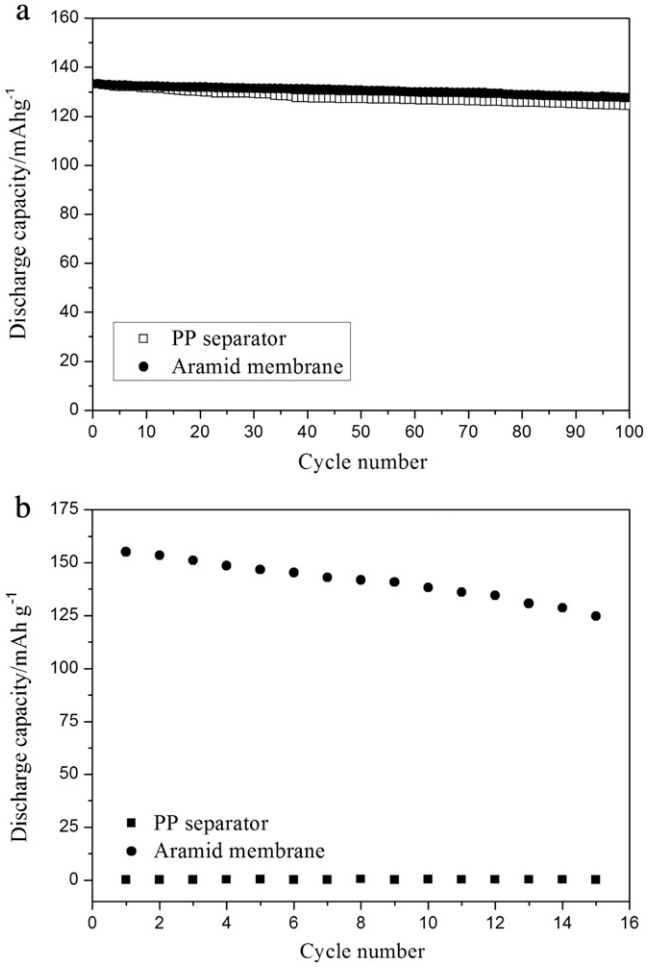


**Fig. 11.** The cycling performance of $LiFePO_4$/Li cells using PP separator and aramid membrane (a) at the room temperature and (b) at 120 °C.

sustain stable charge–discharge curves and afford much better cycling performance than PP separator. Furthermore, the obtained discharge capacities after 15 cycles was around 124.7 mAh $g^{-1}$, indicative of capacity retention ratio of 81%. In order to further verify our hypothesis, we performed OCV changes of $LiFePO_4$/Li cells employing PP separator and aramid membrane during heat exposure at 120 °C. The $LiFePO_4$/Li cell was fully charged at room temperature and was then moved into an oven at 120 °C. As shown in Fig. 12, the OCV of the $LiFePO_4$/Li cell based on PP separator dropped to 0 V only after 40 min. In contrast, the $LiFePO_4$/Li cell using aramid membrane was running well even after 60 min. Clearly, the OCV drop of the cell using PP separator could be explained by the thermal shrinkage of the separator that causes internal short circuits in the cell. It seems that the better thermal stability of aramid membrane would play an important role in improving the elevated temperature characteristics of lithium ion battery. Taking into account inflame retarding properties and safety characteristic, aramid membrane is a promising separator for lithium ion battery even at elevated temperature.

## 4. Conclusions

In the present study, a highly safe and inflame retarding aramid lithium ion battery separator has been prepared via a facile papermaking process. It was demonstrated that aramid membrane possessed better electrolyte wettability, good interfacial compatibility, superior inflame retarding property and thermal resistance than those of conventional PP separator. Moreover, the $LiFePO_4$/Li cell using LiBOB/PC soaked aramid membrane exhibited stable charge–

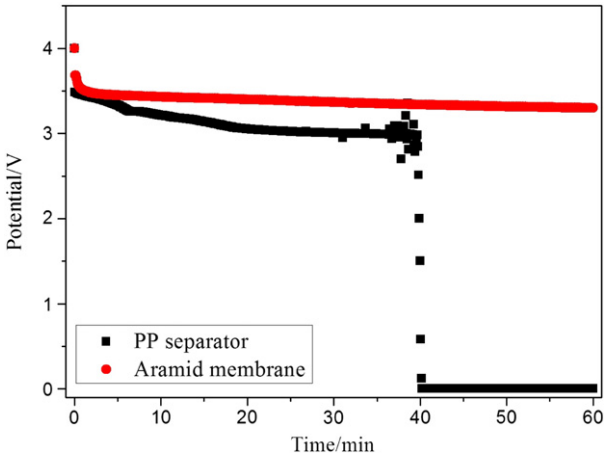


**Fig. 12.** OCV changes of $LiFePO_4$/Li cells employing PP separator and aramid membrane during heat exposure at 120 °C.

discharge profiles and satisfactory cycling performance at an elevated temperature of 120 °C. All characteristics endow aramid membrane a highly promising separator for high-energy lithium ion battery.

## Acknowledgments

The authors express their thanks to the National High Technology Research and Development Program of China (863 Program, No.2013AA050905), the National Program on Key Basic Research Project of China (973 Program) (no. MOST2011CB935700) and the Instrument Developing Project of the Chinese Academy of Sciences (no. YZ201137).

## References

[1] H. Li, Z. Wang, L. Chen, X. Huang, Adv. Mater. 21 (2009) 4593.
[2] J. Hassoun, S. Panero, P. Reale, B. Scrosati, Adv. Mater. 21 (2009) 4807.
[3] M.R. Palacin, Chem. Soc. Rev. 38 (2009) 2565.
[4] G.L. Cui, L. Gu, L.J. Zhi, N. Kaskhedikar, P.A. van Aken, K. Mullen, J. Maier, Adv. Mater. 20 (2008) 3079.
[5] N.A. Kaskhedikar, G.L. Cui, J. Maier, V. Fedorov, V. Makotchenko, A. Simon, Z. Anorg. Allg. Chem. 637 (2011) 523.
[6] G.L. Cui, L. Gu, N. Kaskhedikar, P.A. van Aken, J. Maier, Electrochim. Acta 55 (2010) 985.
[7] Y.J. Xu, X. Liu, G.L. Cui, B. Zhu, G. Weinberg, R. Schlojl, J. Maier, D.S. Su, ChemSusChem 3 (2010) 343.
[8] G. Venugopal, J. Moore, J. Howard, S. Pendalwar, J. Power Sources 77 (1999) 34.
[9] P. Arora, Z. Zhang, Chem. Rev. 104 (2004) 4419.
[10] S.S. Zhang, J. Power Sources 164 (2007) 351.
[11] H.S. Jeong, S.Y. Lee, J. Power Sources 196 (2011) 6716.
[12] J.A. Choi, S.H. Kim, D.W. Kim, J. Power Sources 195 (2010) 6192.
[13] J.H. Park, J.H. Choi, W. Park, D. Ryoo, S.J. Yoon, J.H. Kim, Y.U. Jeong, S.Y. Lee, J. Power Sources 195 (2010) 8307.
[14] H.R. Jung, D.H. Ju, W.J. Lee, X. Zhang, R. Kotek, Electrochim. Acta 54 (2009) 3630.
[15] D. Fu, B. Luan, A. Steve, N.M. Bureau, J.I. Davidson, J. Power Sources 206 (2012) 328.
[16] C. Fausto, M.L. Focarete, J. Hassoun, I. Meschinia, B. Scrosati, Energy Environ. Sci. 4 (2011) 921.
[17] P. Carol, P. Ramakrishnan, B. John, G. Cheruvally, J. Power Sources 196 (2011) 10159.
[18] H.S. Jeong, E.S. Choi, J.H. Kim, S.Y. Lee, Electrochim. Acta 56 (2011) 5202.
[19] H.S. Jeong, J.H. Noh, C.G. Hwang, S.H. Kim, S.Y. Lee, Macromol. Chem. Phys. 211 (2010) 420.
[20] H.S. Jeong, J.H. Kim, S.Y. Lee, J. Mater. Chem. 20 (2010) 9180.
[21] C. Yang, Z. Jia, Z. Guan, L. Wang, J. Power Sources 189 (2009) 716.
[22] T.H. Cho, M. Tanaka, H. Ohnish, Y. Kondo, M. Yoshkazu, T. Nakamura, T. Sakai, J. Power Sources 195 (2010) 4272.
[23] W. Qi, C. Lu, P. Chen, L. Han, Q. Yu, R.Q. Xu, Mater. Lett. 66 (2012) 239.
[24] X.S. Huang, J. Solid State Electrochem. 15 (2011) 649.
[25] Y.J. Kim, C.H. Ahn, M.B. Lee, M.S. Choi, Mater. Chem. Phys. 127 (2011) 137.
[26] Y.E. Miao, G.N. Zhu, H.Q. Hou, Y.Y. Xia, T.X. Liu, J. Power, Sources 226 (2013) 82.
[27] Y.S. Lee, Y.B. Jeong, D.W. Kim, J. Power Sources 195 (2010) 6197.
[28] H.S. Jeong, S.C. Hong, S.Y. Lee, J. Membr. Sci. 364 (2010) 177.
[29] Z.Y. Cui, Y.Y. Xu, L.P. Zhu, J.Y. Wang, B.K. Zhu, Ionics 15 (2009) 469.
[30] C.B. Wang, S.J. Ying, Z.G. Xiao, Acta Polym. Sin. 12 (2011) 1419.
[31] M. Szpieg, H. Wysocki, L.E. Asp, J. Compos. Mater. 46 (2012) 1503.
[32] E. Santos, H. Schulz, M. Figueiredo, TAPPI J. 4 (2005) 20.
[33] Y.J. Wu, C.S. James, L. Vincent, J. Appl. Polym. Sci. 86 (2002) 1149.
[34] T. Amornsakchaia, B. Sinpatanapana, S. Bualek-Limcharoena, Polymer 40 (1999) 2993.
[35] J. Lee, R.M. Broughton, S.D. Worley, Eng. Fibers Fabr. 4 (2007) 25.
[36] W.J. Li, C.T. Laurencin, E.J. Caterson, J. Biomed. Mater. Res. 60 (2002) 613.
[37] J. Song, M.H. Ryou, B. Son, J.N. Lee, D.J. Lee, Y.M. Lee, J.W. Choi, J.K. Park, Electrochim. Acta 85 (2012) 524.
[38] J.J. Zhang, Z.H. Liu, Q.S. Kong, C.J. Zhang, S.P. Pang, L.P. Yue, X.J. Wang, J.H. Yao, G.L. Cui, ACS Appl. Mater. Interfaces 5 (2013) 128.
[39] J. Ding, Y. Kong, P. Li, J.R. Yang, J. Electrochem. Soc. 159 (2012) 1474.
[40] N. Wu, Q. Cao, X.Y. Wang, Q.Q. Chen, Solid State Ionics 203 (2011) 42.
[41] K.H. Hwang, B.M. Kwon, H.S. Byun, J. Membr. Sci. 378 (2011) 111.
[42] L.C. Zhang, X. Sun, Z. Hu, C.C. Yuan, C.H. Chen, J. Power Sources 204 (2012) 149.
[43] S.J. Chun, E.S. Choi, E.H. Lee, J.H. Kim, S.Y. Lee, S.Y. Lee, J. Mater. Chem. 22 (2012) 16618.
[44] T. Feng, F. Wu, C. Wu, X.D. Wang, G.S. Feng, H.Y. Yang, Solid State Ionics 221 (2012) 28.
[45] J.J. Zhang, Q. Ji, P. Zhang, Y.Z. Xia, Q.S. Kong, Polym. Degrad. Stab. 95 (2010) 1211.
[46] F. Wu, T. Feng, Y. Bai, C. Wu, L. Ye, Z.G. Feng, Solid State Ionics 180 (2009) 677.
[47] M. Ulaganathan, R. Nithya, S. Rajendran, S. Raghu, Solid State Ionics 218 (2012) 7.
[48] S.H. Kim, K.H. Choi, S.J. Cho, E.H. Kil, S.Y. Lee, J. Mater. Chem. A 1 (2013) 4949.
[49] J.J. Zhang, L.P. Yue, Q.S. Kong, Z.H. Liu, X.H. Zhou, C.J. Zhang, S.P. Pang, X.J. Wang, J. Electrochem. Soc. 160 (2013) 769.
[50] J.L. Hao, G.T. Lei, Z.H. Li, L.J. Wu, Q.Z. Xiao, L. Wang, J. Membr. Sci. 428 (2013) 11.
[51] W. Qi, C. Lu, P. Chen, L. Han, Q. Yu, R.Q. Xu, Mater. Lett. 66 (2012) 240.
[52] Y. Wang, H.Y. Zhan, J. Hu, Y. Liang, S.S. Zeng, J. Power Sources 189 (2009) 616.
[53] M.H. Ryou, Y.M. Lee, J.K. Park, J.W. Choi, Adv. Mater. 23 (2011) 3066.
[54] K.S. Liu, X. Yao, L. Jiang, Chem. Soc. Rev. 39 (2010) 3240.
[55] Z.H. Liu, W. Jiang, Q.S. Kong, C.J. Zhang, P.X. Han, X.J. Wang, J.H. Yao, G.L. Cui, Macromol. Mater. Eng. (2012), http://dx.doi.org/10.1002/mame.201200158.
[56] R.S. Villar, J.I. Paredes, A.A. Martines, Therm. Anal. Calorim. 70 (2002) 37.
[57] W. Jiang, Z.H. Liu, Q.S. Kong, J.H. Yao, C.J. Zhang, P.X. Han, G.L. Cui, Solid State Ionics 232 (2013) 44.
[58] J.J. Zhang, Q. Ji, F.J. Wang, L.W. Tan, Y.Z. Xia, Polym. Degrad. Stab. 97 (2012) 1034.
[59] J.J. Zhang, Q. Ji, X.H. Shen, Y.Z. Xia, L.W. Tan, Q.S. Kong, Polym. Degrad. Stab. 96 (2011) 936.
[60] A. Korematsu, T. Furuzono, A. Kishida, Macromol. Mater. Eng. 290 (2005) 66.
[61] K. Xu, Chem. Rev. 104 (2004) 4303.
[62] D. Djian, F. Alloin, S. Martinet, H. Lignier, J.Y. Sanchez, J. Power Sources 172 (2007) 416.
[63] C.J. Zhang, X. He, Q.S. Kong, H. Li, H. Hu, H.B. Wang, L. Gu, L. Wang, G.L. Cui, L.Q. Chen, CrystEngComm 14 (2012) 4344–4349.
[64] Y.H. Huang, R.I. Dass, Z.L. Xing, J.B. Goodenough, Science 312 (2006) 254–257.